Supporting Information for:

Structural Resolution and Mechanistic Insight into Hydrogen Adsorption in Flexible ZIF-7

Ryan A. Klein,[a,b] Sarah Shulda,[a] Philip A. Parilla,[a] Pierre Le Magueres,[c] Rachelle K. Richardson,[d] William Morris,[d] Craig M. Brown,[b,e] C. Michael McGuirk*[f]

[a] *Material, Chemical, and Computational Sciences Directorate, National Renewable Energy Laboratory, Golden Colorado 80401, USA*
[b] *Center for Neutron Research, National Institute of Standards and Technology, Gaithersburg, Maryland 20899, USA*
[c] *Rigaku Americas Corporation, 9009 New Trails Drive, The Woodlands, TX 77381, United States*
[d] *NuMat Technologies, 8025 Lamon Avenue, Skokie, Illinois 60077, United States*
[e] *Department of Chemical and Biomolecular Engineering, University of Delaware, Newark, Delaware 19716, USA*
[f] *Department of Chemistry, Colorado School of Mines, Golden, Colorado 80401, USA*

Chemical Science

Table of Contents

Full experimental details

General considerations: Reagents and solvents were purchased from commercial suppliers‡ at reagent grade purity or higher and were used as received. Benzimidazole (99%), zinc nitrate hexahydrate (98%), ammonium hydroxide solution in water (28%–30%), cadmium perchlorate hydrate and all solvents were purchased from Sigma Aldrich. Ultrahigh purity H_2 (99.9999%) and He (99.9999%) gasses were purchased from Matheson and was used for the adsorption isotherm measurements.

Synthesis and activation of ZIF-7: Similar to the reported procedure,[1,2] a 50 mL round-bottom flask was charged with $Zn(NO_3)_2{\cdot}6H_2O$ (0.900 g, 3.00 mmol, 1 eq) and 10 mL ethanol. The mixture was sonicated until all the solids dissolved. A separate 100 mL round-bottom flask was charged with benzimidazole (0.72 g, 6.0 mmol, 2 eq.) and 30 mL ethanol, to which 28–30% aqueous NH_3 (2.8 g, 48 mmol NH_3, 16 eq.) was added and the mixture was equipped with a stir bar. The $Zn(NO_3)_2{\cdot}6H_2O$/ethanol solution was then added to the stirring benzimidazole/NH_3/ethanol mixture. Precipitation was observed immediately upon mixing. The suspension was subsequently stirred at room temperature (~25 °C) for 0.5 h. The suspension was then filtered through filter paper and thoroughly washed with excess fresh ethanol, followed by vacuum drying on the filter paper for 5 min. The white powder was then transferred to a vial and activated under dynamic vacuum at 230 °C for 48 h. Upon cooling to room temperature, the activated powder was subsequently immersed in fresh, excess ethanol for 72 h. For all gas adsorption measurements, the solid was again filtered over filter paper, washed with excess ethanol, and activated overnight (~16 h) at 100 °C under dynamic vacuum. Activated ZIF-7 was obtained as a white solid.

Synthesis and crystal growth of activated CdIF-13: The synthesis of CdIF-13 followed a previously reported procedure.[2] Note that the reagent $Cd(ClO_4)_2{\cdot}xH_2O$ is an oxidant and is acutely toxic. Necessary precautions for safe handling should be taken.

A 20 mL scintillation vial was charged with $Cd(ClO_4)_2{\cdot}xH_2O$, benzimidazole, and 10 mL of *N*,*N*-dimethylformamide. The vial was capped and then sonicated until the reagents dissolved to yield a clear, colorless solution. This was then heated to 130 °C at a rate of 5 °C min^{-1} in a temperature-programmable oven, and held at this temperature for 24 h. Afterwards, the sample was slowly cooled to room temperature by turning the oven off and keeping the oven door sealed. Colorless crystals of CdIF-13 were recovered by vacuum filtration and washed with excess *N*,*N*-dimethylformamide. The crystals were dried under active vacuum at room temperature and then placed in a 20 mL scintillation vial filled with 15 mL dichloromethane and left for 24 h. After 24 h, the polycrystalline powder was collected via vacuum filtration, and then placed in 15 mL fresh dichloromethane. This procedure was repeated a total of 3 times to affect the solvent exchange. Small single crystals of CdIF-13·*x*DCM were removed from the mother liqueur. Serendipitous evaporation of the DCM solvent molecules at room temperature from the crystals resulted in a crystal-to-crystal phase transformation to yield the single crystal of activated CdIF-13.

Single crystal X-ray diffraction measurements and structure solution of activated CdIF-13: Crystals of activated CdIF-13 (colorless crystal) were taken out of their mother liquor and immediately placed into a drop of Paratone oil. A tiny crystal, with dimensions 0.015 mm × 0.041 mm × 0.048 mm, was secured within a thin layer of Paratone oil in a fiber loop micromount. The SCXRD data were collected at 100 K using a Rigaku XtaLAB Synergy-S X-ray diffractometer equipped with a HyPix-6000HE hybrid photon counting (HPC) detector and microfocused Cu-Kα radiation (λ = 1.54184 Å). To ensure completeness and desired redundancy, the data collection strategy was calculated using CrysAlis^{Pro}.[3] Data collection and data processing were also performed in CrysAlis^{Pro}. Using the SCALE3 ABSPACK scaling algorithm,[4] empirical absorption corrections were applied to the data. The structure was solved *via* intrinsic phasing methods using ShelXT and refined using ShelXL in the Olex2 graphical user interface.[5–6] The final

structural refinements included anisotropic temperature factors on all non-hydrogen atoms. Hydrogen atoms were attached via the riding model at calculated positions using suitable HFIX commands.

Details of gas adsorption isotherm measurements: The hydrogen capacity isotherms were collected using the manometric method.[7] In a helium-filled glove box with less than 0.1 ppm H_2O and O_2, 1.62 g of ZIF-7 crystalline powder was loaded into the sample holder. The sample holder contains a manual valve that allows the sample to be isolated from the environment for air-free transfer. The sample holder was transferred, without exposure to air, from the glovebox to a degas TPD instrument where the sample was heated from room temperature to 200 °C at 5 °C/min under turbopump vacuum with base pressure 10^{-8} mmHg and held at 200 °C for 6 hours. After degassing, the sample, under vacuum, was transferred to the PCTPro 2000 instrument. The head space above the sample holder isolation valve was evacuated prior to beginning the gas capacity experiments. The PCTPro has been modified for increased temperature control of the reference and sample volumes and the sample temperature is controlled to within 0.01 K via an ARS cryo system with a cryogenic head modified to accommodate the sample holder.

The sample sorption capacity is determined via exposing the sample to a series of hydrogen pressures where the number of moles of hydrogen introduced at each step is calculated from measuring the pressure in a well-defined *reference volume* with calibrated volume and at known temperature. Between this reference volume and sample volume, a pneumatic valve is opened, and the resultant pressure is measured for the combined volumes, termed the *total volume*. A schematic highlighting the reference and total volumes is provided in figure S1. The combined or total volume is determined by an equivalent experiment using helium, which is assumed to have negligible adsorption on the sample at 303 K. After allowing the sample to come to equilibrium with the gas, the pressure is measured. Based on the calibrated volumes and measured temperature profile of those volumes plus the calculated moles, pressures measured and found to be lower than expected for the number of moles of hydrogen gas introduced are assumed to result from adsorption onto the sample while pressures found to be higher than expected are assumed arise from gas desorption from the sample. Gas capacity was calculated from the pressure data using a mole-balance of the gas phase at each step. A real equation of state used for hydrogen and helium with the compressibility factor was determined from calculations using GASPAK.[8]

Details of adsorption isotherm fitting: The isoexcess enthalpy of adsorption was determined via a discretized form of the Clausius-Clapeyron equation which approximates the isosteric enthalpy of adsorption from two isotherms as a function of moles sorbed (Equation 1),

$$\Delta h_{st} = RT_1T_2\left(\frac{ln\left(P_2/P_1\right)}{T_2 - T_1}\right)_{n_{ex}} \qquad \text{(Eq. S1)}$$

where Δh_{st} is the isosteric enthalpy of adsorption, R is the universal gas constant, T_1 and P_1 are the temperature and pressure of the first isotherm and T_2 and P_2 correspond to the second isotherm at the same excess mole loading, as indicated by n. Derivation and details on the use of the equation can be found elsewhere.[8,9,10] The Clausius-Clapeyron equation assumes that the isotherms are in terms of absolute sorption, which cannot be unambiguously measured. Typically, as is the case herein, isotherm measurements determine excess sorption. To avoid introducing unknown error into the calculations, the excess data was used directly in the enthalpy of adsorption approximation and was not converted to absolute adsorption. Following convention when using excess sorption for the Clausius-Clapeyron approximation, the values reported here are referred to as *isoexcess* enthalpies of adsorption.[11,11]

Determining P_1 and P_2 at the same mole loading necessitates fitting the experimental data. The dense and open phase segments of each isotherm were separately fit with a Langmuir-Freundlich isotherm model, (Equation 2),

$$n = \frac{a(bP)^c}{1 + (bP)^c} \quad \text{(Eq. S2)}$$

where *n* is the moles sorbed, a, b, and c are fit coefficients, and P is pressure. Only the adsorption data was fit, not the desorption data. The adsorption isotherm for the dense and open phases are concave down, as expected, with an inflection point at the start and end of the step region. Thus, it is possible to robustly determine the segments of the isotherms corresponding to the dense and open phase from evaluating the second derivative of the isotherms. The resulting fits are provided in Figs. S3–S5 and the corresponding fit coefficients in Table S1. The isotherm fits were used with the Clausius-Clapeyron equation to solve for the isoexcess enthalpy of adsorption using the 100 K and 110 K isotherm pair and the 110 K and 125 K pair as a function of excess moles adsorbed. The enthalpy results are provided in Fig. S6. We fit both the pre-step and post-step regimes because, as the structure changes, new sites become available, and the energetics of the existing sites may change. We used the same equation to fit both regimes because it accounts for the for the distribution of adsorption site energies, and it is applicable to materials with both homogeneous adsorption sites and heterogeneous adsorption sites over a wide pressure range.[12]

Details of powder neutron diffraction measurements: 2.38 g of pristine ZIF-7 crystalline powder were heated to 200 °C and evacuated using a turbo-molecular vacuum pump (≈ 10^{-6} mmHg) over 3 days. The powder was loaded into a vanadium sample can (inner diameter = 9.2 mm) in a helium-filled glovebox equipped with water and oxygen sensors. The sample can was sealed using an indium O-ring and a lid with a capillary gas line and a packless valve, and then removed from the glovebox and mounted onto a bottom-loading closed-cycle refrigerator. The sample was evacuated at room temperature, cooled to 7 K, and a powder neutron diffraction (PND) pattern was measured on the high-resolution powder diffractometer BT-1 at the National Institute of Standards and Technology Center of Neutron Research (NCNR) for ≈ 24 h. A Ge(311) monochromator (in-pile columniation of 60') generated a neutron wavelength of λ = 2.0772 Å. After the initial measurement of the activated material, the sample was warmed to room temperature, dosed with a known volume of D_2 gas corresponding to 0.7 equivalents of D_2 molecules per Zn atom in the ZIF-7 framework, cooled slowly to 11 K, and measured for ≈ 24 h.

For the high-pressure measurements, 2.9 g ZIF-7 were loaded into a pressure-rated aluminum can under a helium environment. The sample was loaded into a closed-cycle refrigerator. The sample was evacuated under dynamic vacuum at room temperature, cooled to 74 K and then dosed with D_2 gas to a pressure of 29.8 bar D_2. A PND pattern was collected over ≈ 24 h using the same instrument configuration as before. The sample was then heated, and the pressure was monitored. Additional PND patterns were collected at temperature and pressure conditions of T = 99 K, P = 31.0 bar D_2 (collection time ≈ 24 h); T = 128 K, P = 28.6 bar D_2 (collection time ≈ 20 h); T = 146 K, P = 28.8 bar D_2 (collection time ≈ 20 h); and T = 194 K, P = 29.2 bar D_2 (collection time ≈ 20 h).

Powder neutron diffraction data analysis: The powder neutron diffraction data were analyzed using the Topas Academic software package[13] and EXPGUI/GSAS.[14,15] Initial Pawley fits were used to extract the unit cell parameters for the activated and gas-dosed structures.[16] We compare the unit cell parameters found herein with selected structures published in the literature in Table S2.[17] After successful Pawley fitting, we performed simulated annealing in real space[18] using rigid body models for the benzimidazolate ligands to best locate their positions and orientations to obtain the corresponding crystal structures. Full occupancies

of framework atoms were assumed. Bond length and angle restraints were employed to maintain an approximately tetrahedral geometry for the Zn atoms with Zn–N bond lengths of ≈ 2.0 Å.[19] Subsequently a full Rietveld refinement yielded the crystal structure for activated ZIF-7 (Fig. S2).[20] This structure was then used as a starting model for the framework in the analysis of the gas-dosed data sets while the structure was in the dense, triclinic phase. A super-atom approach was used to model the D_2 gas molecules.[21–22] This approach, which accounts for quantum disorder of the D_2 molecule in the structure, treats the molecules as point scatterers with doubled occupancy and large isotropic thermal parameters to mimic the orientational average from the $D_{\infty h}$ molecule when physisorbed. Similarly, simulated annealing in real space followed by a systematic Rietveld refinement of the entire model yielded the structure of the D_2-dosed frameworks (Figs. S2–S7). For the high-pressure measurements, the diffraction from the aluminum sample can is evident in the patterns. The reflections for the aluminum phase were fit using a Pawley refinement (effects from texture and geometry preclude a full Rietveld refinement for the Al sample can). The Pawley fitting process revealed a monoclinic unit cell for ZIF-7 in the 74 K and 99 K data sets, different from the activated phase or the parent trigonal structure for the water solvated phase.[20] The structure crystallizes in the $P2_1/n$ space group, similar to the dimethylformamide (DMF) and dichloromethane solvated crystal structures found for the isostructural Cd congener, CdIF-13.[2] The refined unit cell parameters for these compounds are tabulated in Table S2. The unit cell parameters for ZIF-7 at ≈ 77 K and 30 bar D_2 conditions was most similar to those reported for the DCM solvated phase of CdIF-13. As such, the ligand orientations in the DCM solvated phase were used as approximate starting positions for the ligand positions in the ZIF-7 Rietveld refinement. It should be noted that the activated structure naturally transforms into this open phase with gate-type motion of the ligands.

Details of pelletization and measurements on resulting pellets: 5 mass % polyvinylpyrrolidone (PVP) binder was added to solvent exchanged ZIF-7 (MeOH approximately 30 mass %). Pellets were pressed at pressures of 10,000 psi, 30,000 psi, and 50,000 psi. Activation of ZIF-7 pellets was performed in under dynamic vacuum at 150 ˚C. Upon activation, PXRD patterns were collected for each pellet (Fig. S13). The density of each pellet was measured by determining the volume of each pellet and mass following activation was used. A crystal density of 1.39 g/cc was used for the open form. CO_2 adsorption-desorption isothermal measurements were conducted at 298 K using a micromeritics 2050 instrument.

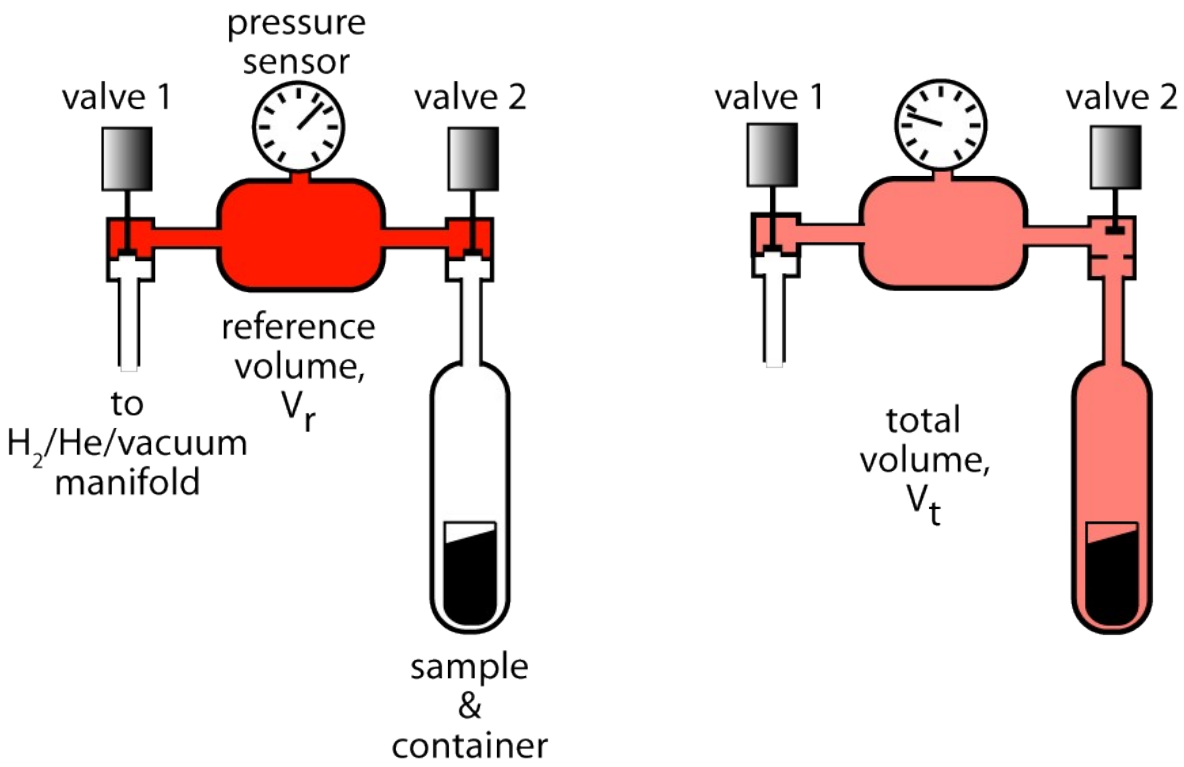

Figure S1. Schematic highlighting the reference volume and total volume used in the manometric gas capacity measurements.

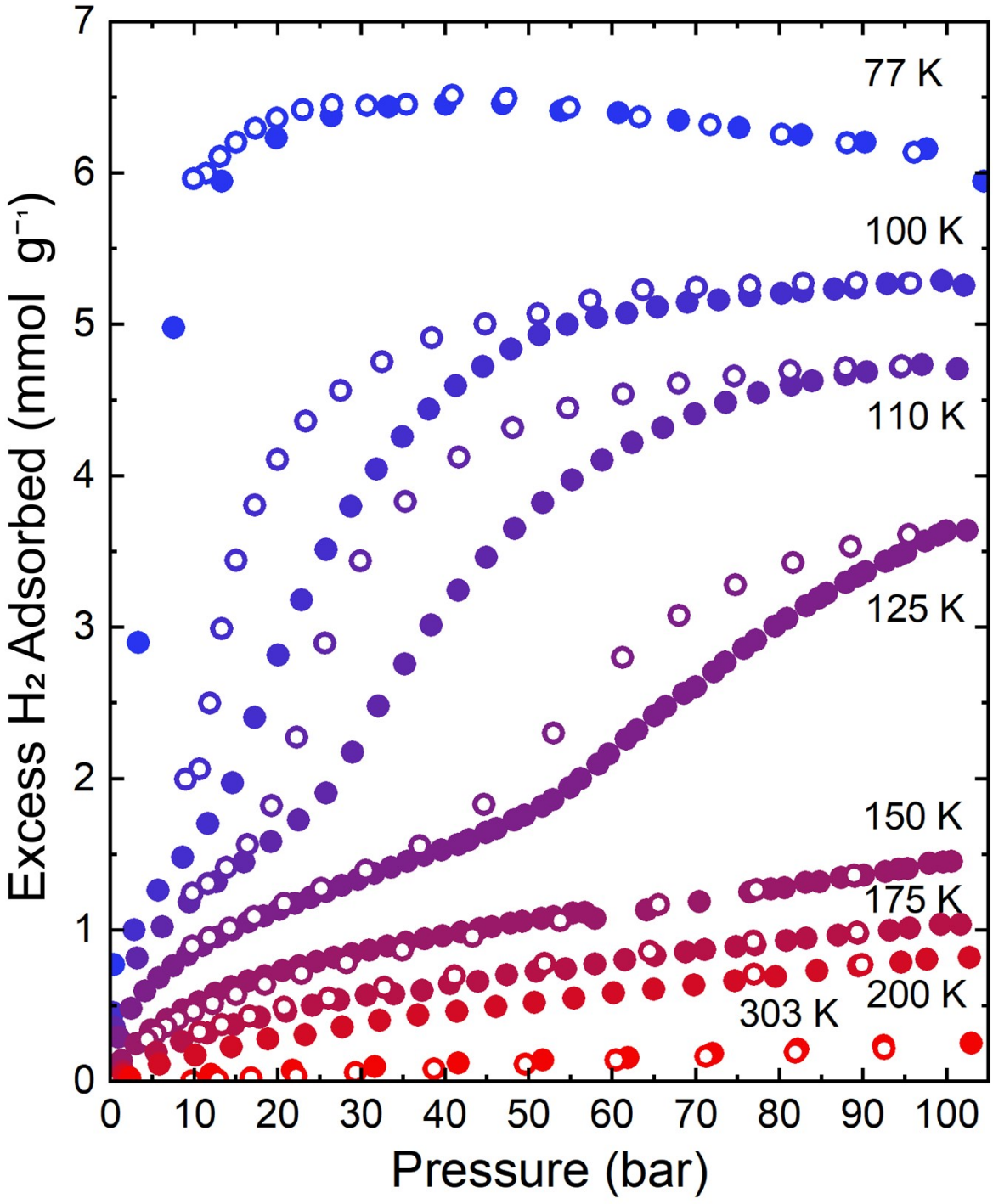

Figure S2. Hydrogen excess adsorption isotherm data for ZIF-7. The temperatures at which the data were collected are listed at the right of the figure next to each data set. The color of each data set is meant to indicate temperature but the change in color is not proportional to the temperature change. Spurious data points in the 150 K data set between 60 bar and 80 bar measured upon adsorption, caused by temporary temperature control issues, are not included here.

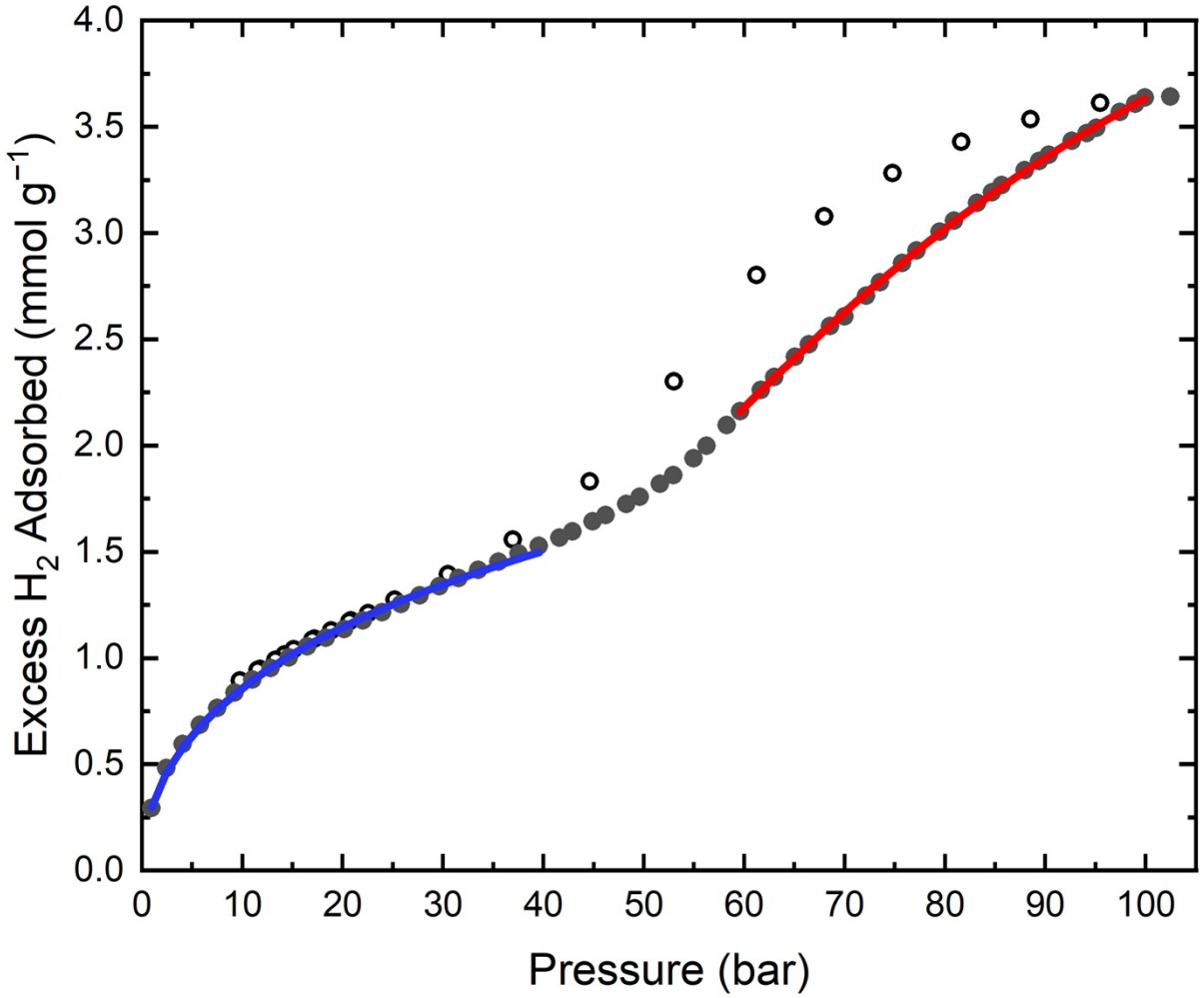

Figure S3. Hydrogen excess adsorption isotherm data for ZIF-7 measured at 125 K upon adsorption (closed symbols) and desorption (open symbols). The colored curves represent the single-site Freundlich-Langmuir fits to the data in the dense (blue curve) and open (red curve) phases. The fit curves are truncated within the measured pressure range relevant to the phases. Only the adsorption data are fit. The fit parameters are tabulated in Table S1. $\chi^2 = 5.43 \times 10^{-9}$ for the dense phase; $\chi^2 = 1.88 \times 10^{-7}$ for the open phase.

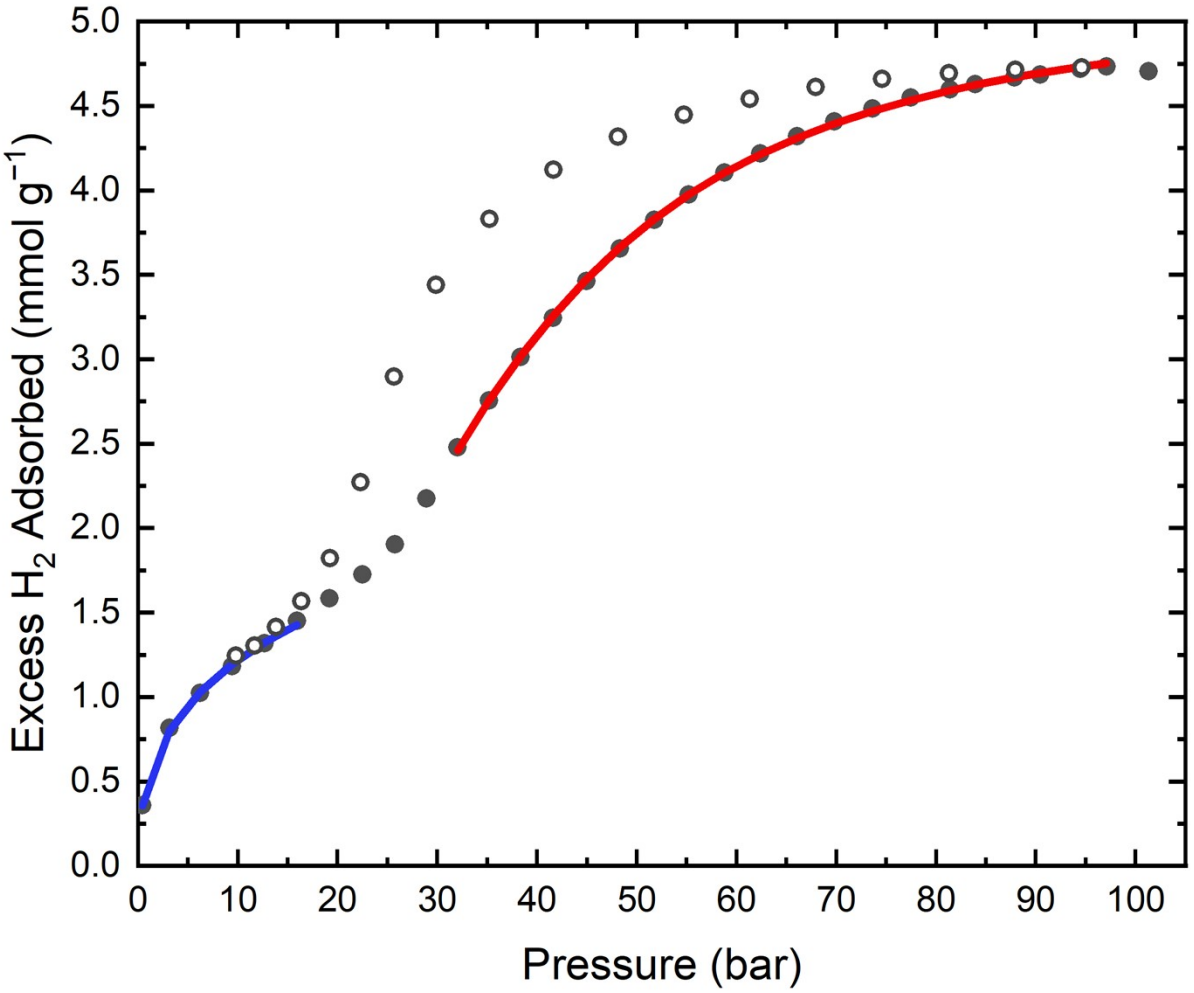

Figure S4. Hydrogen excess adsorption isotherm data for ZIF-7 measured at 110 K upon adsorption (closed symbols) and desorption (open symbols). The colored curves represent the single-site Freundlich-Langmuir fits to the data in the dense (blue curve) and open (red curve) phases. The fit curves are truncated within the measured pressure range relevant to the phases. Only the adsorption data are fit. The fit parameters are tabulated in Table S1. $\chi^2 = 1.16 \times 10^{-8}$ for the dense phase; $\chi^2 = 2.31 \times 10^{-8}$ for the open phase.

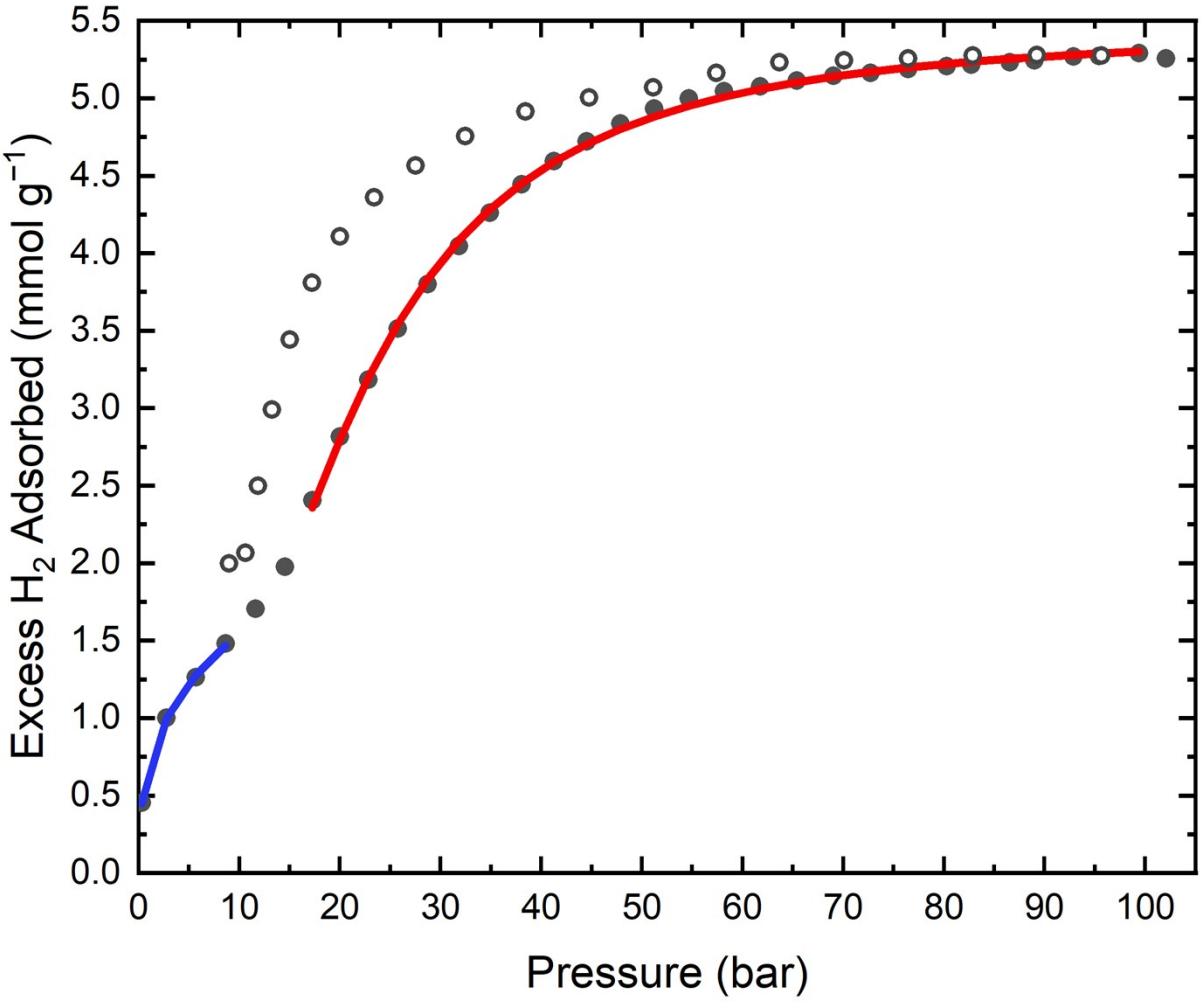

Figure S5. Hydrogen excess adsorption isotherm data for ZIF-7 measured at 100 K upon adsorption (closed symbols) and desorption (open symbols). The colored curves represent the single-site Freundlich-Langmuir fits to the data in the dense (blue curve) and open (red curve) phases. The fit curves are truncated within the measured pressure range relevant to the phases. Only the adsorption data are fit. The fit parameters are tabulated in Table S1. $\chi^2 = 4.23 \times 10^{-8}$ for the dense phase; $\chi^2 = 1.08 \times 10^{-8}$ for the open phase.

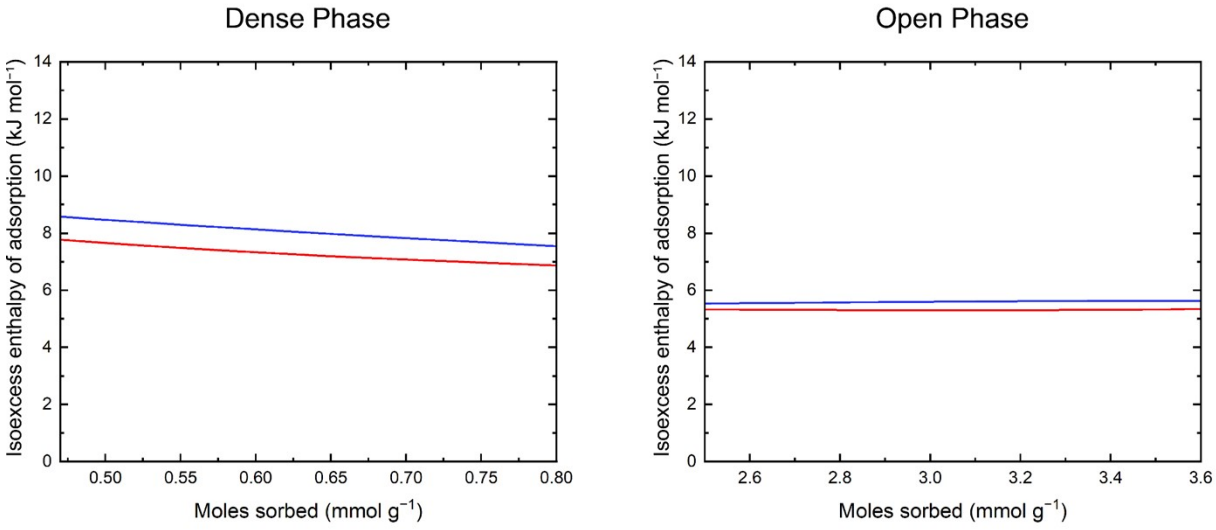

Figure S6. The isoexcess enthalpy of adsorption as a function of H_2 loading for ZIF-7 based on the single-site Freundlich-Langmuir fits to the isothermal data at 100 K and 110 K (red curve) and at 110 K and 125 K (blue curve). The data for the dense phase are shown in the plot on the left while the data for the open phase are shown in the plot on the right.

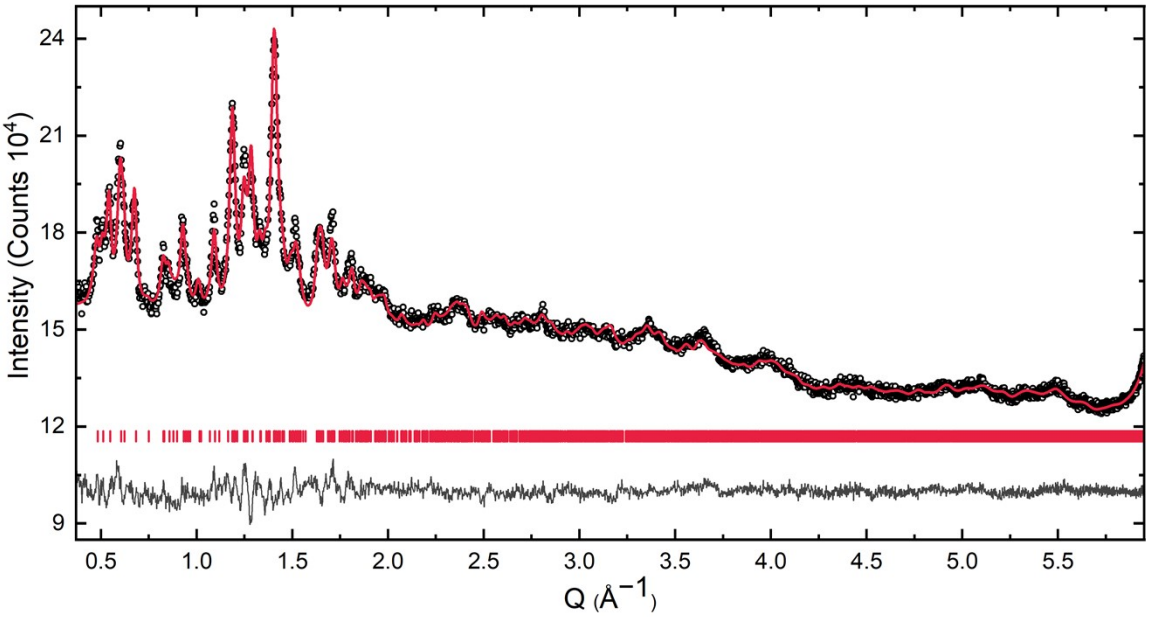

Figure S7. Rietveld refinement of the powder neutron diffraction pattern of activated ZIF-7 at T = 7 K, λ = 2.0772 Å. R_{wp} = 0.977 %, R_p = 0.837 %, R_{exp} = 0.824 %, GOF = 1.186. The black circles, red curve, grey curve, and vertical tick marks denote the raw data, the Rietveld refinement curve, the difference curve, and the *hkl* positions, respectively.

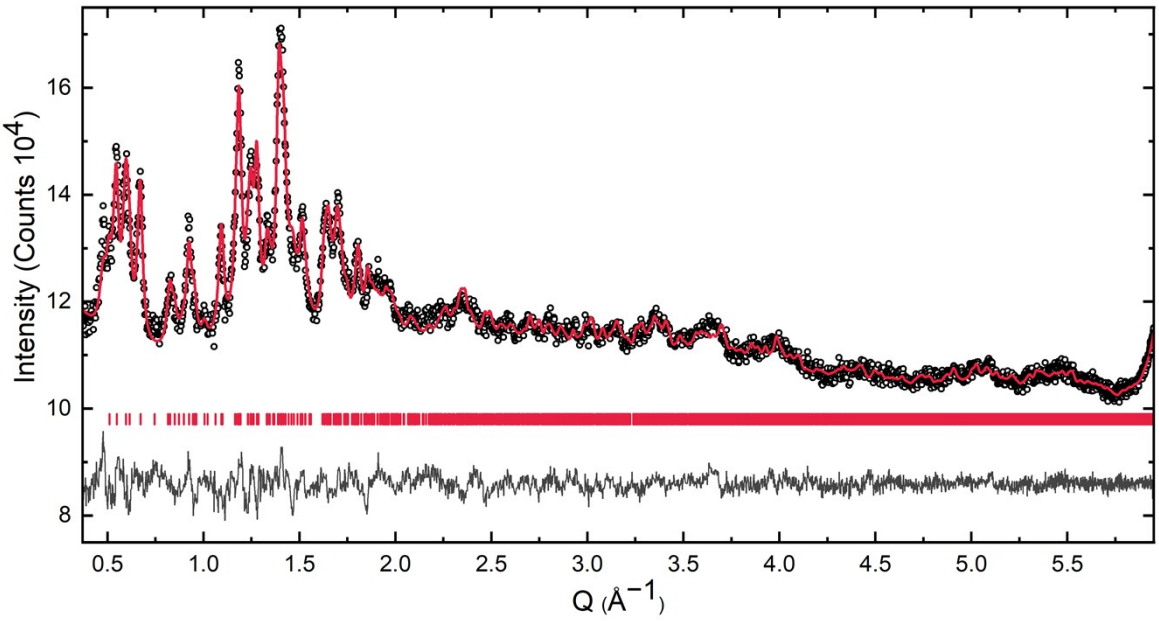

Figure S8. Rietveld refinement of the powder neutron diffraction pattern of activated ZIF-7 dosed with 0.7 eq. D_2 per Zn ion, obtained at T = 11 K, λ = 2.0772 Å. R_{wp} = 1.086 %, R_p = 0.944 %, R_{exp} = 0.934 %, GOF = 1.163. The black circles, red curve, grey curve, and vertical tick marks denote the raw data, the Rietveld refinement curve, the difference curve, and the *hkl* positions, respectively.

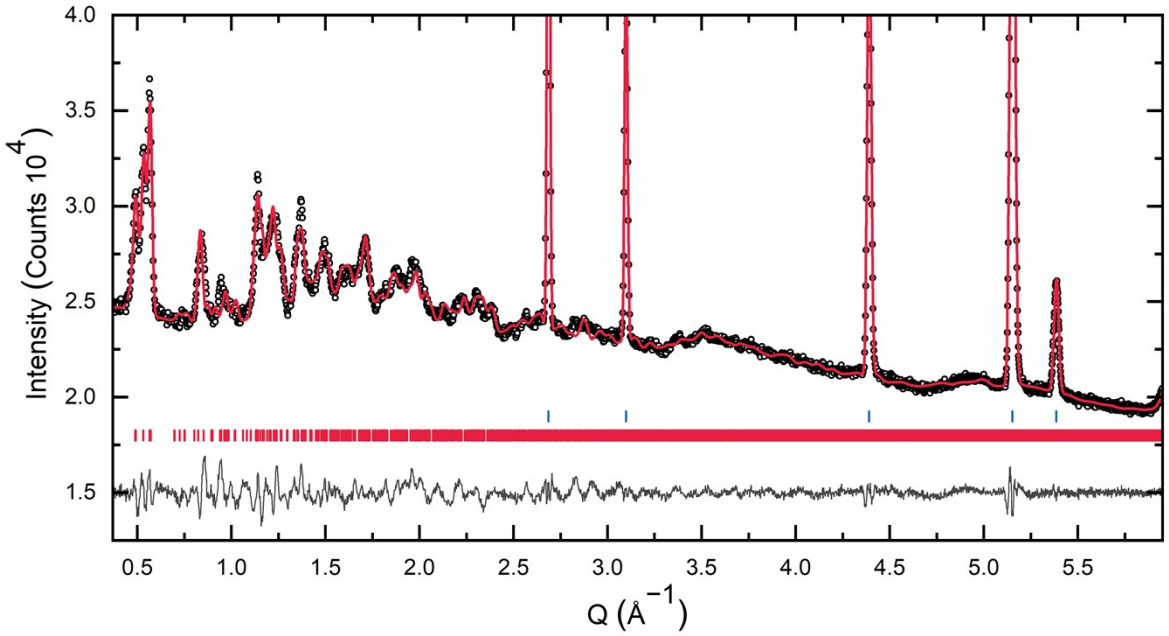

Figure S9. Rietveld refinement of the powder neutron diffraction pattern of ZIF-7 obtained at T = 74 K, P = 29.8 bar D_2, λ = 2.0772 Å. R_{wp} = 1.093 %, R_p = 0.899 %, R_{exp} = 0.652 %, GOF = 1.676. The black circles, red curve, grey curve, and red and blue vertical tick marks denote the raw data, the Rietveld refinement curve, the difference curve, and the *hkl* positions for ZIF-7 and aluminum, respectively.

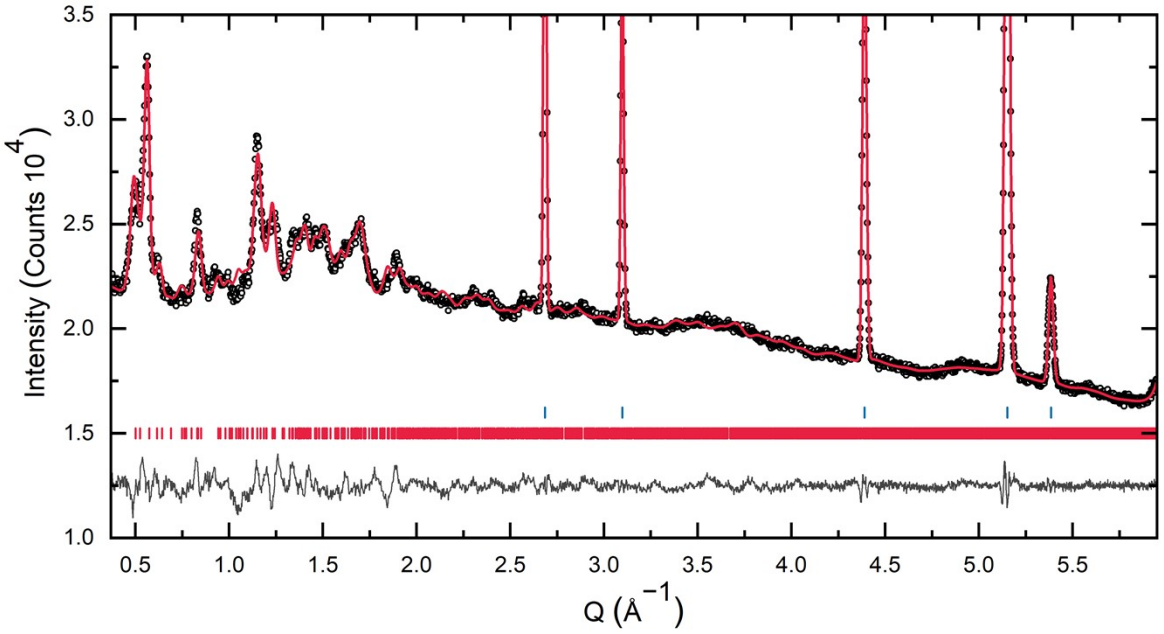

Figure S10. Rietveld refinement of the powder neutron diffraction pattern of ZIF-7 obtained at T = 99 K, P = 31.0 bar D_2, λ = 2.0772 Å. R_{wp} = 1.079 %, R_p = 0.894 %, R_{exp} = 0.700 %, GOF = 1.542. The black circles, red curve, grey curve, and red and blue vertical tick marks denote the raw data, the Rietveld refinement curve, the difference curve, and the *hkl* positions for ZIF-7 and aluminum, respectively.

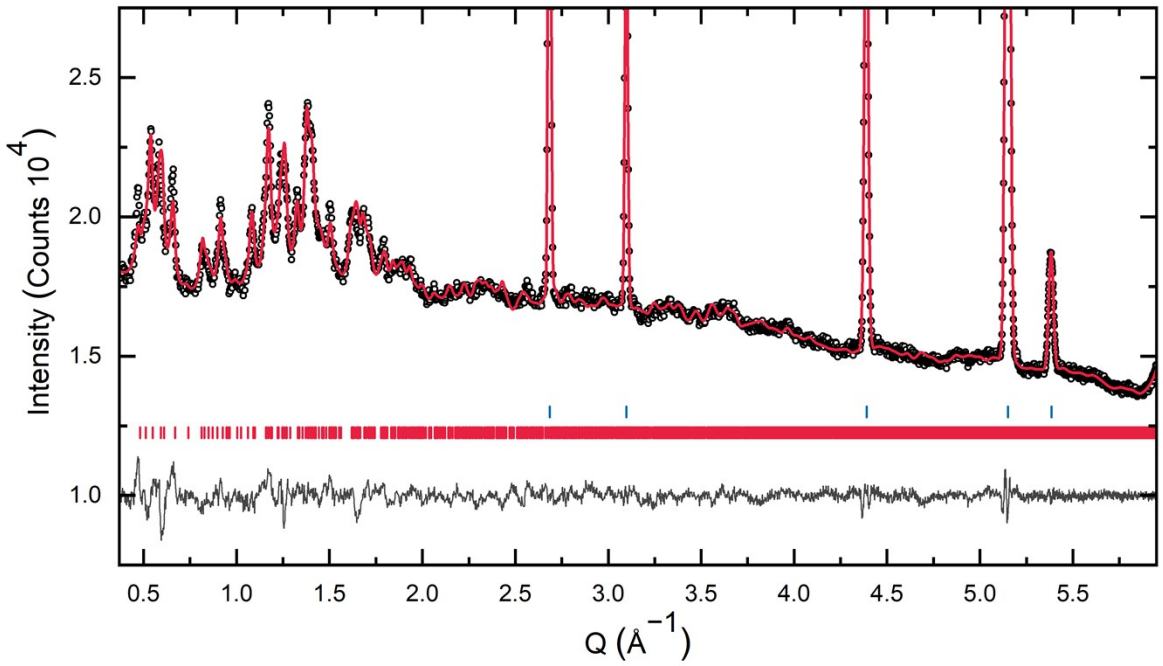

Figure S11. Rietveld refinement of the powder neutron diffraction pattern of ZIF-7 obtained at T = 128 K, P = 28.6 bar D_2, λ = 2.0772 Å. R_{wp} = 1.087 %, R_p = 0.901 %, R_{exp} = 0.770 %, GOF = 1.412. The black circles, red curve, grey curve, and red and blue vertical tick marks denote the raw data, the Rietveld refinement curve, the difference curve, and the *hkl* positions for ZIF-7 and aluminum, respectively.

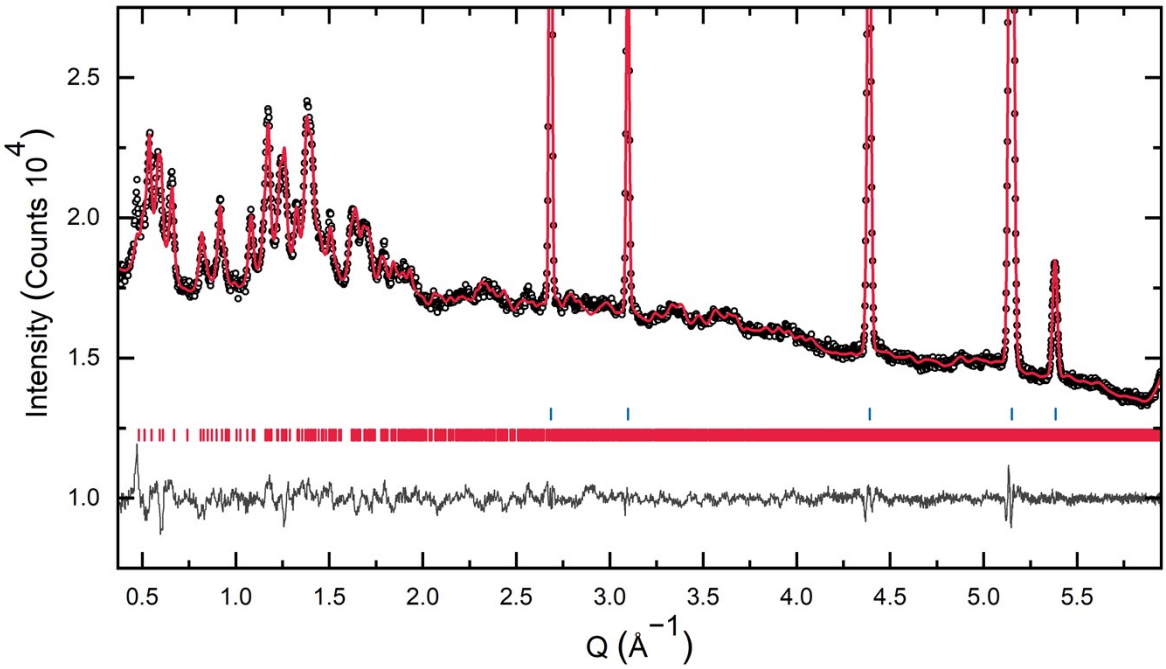

Figure S12. Rietveld refinement of the powder neutron diffraction pattern of ZIF-7 obtained at T = 146 K, P = 28.8 bar D_2, λ = 2.0772 Å. R_{wp} = 1.068 %, R_p = 0.872 %, R_{exp} = 0.768 %, GOF = 1.390. The black circles, red curve, grey curve, and red and blue vertical tick marks denote the raw data, the Rietveld refinement curve, the difference curve, and the *hkl* positions for ZIF-7 and aluminum, respectively.

Figure S13. Rietveld refinement of the powder neutron diffraction pattern of ZIF-7 obtained at T = 195 K, P = 29.2 bar D_2, λ = 2.0772 Å. R_{wp} = 1.018 %, R_p = 0.841 %, R_{exp} = 0.725 %, GOF = 1.404. The black circles, red curve, grey curve, and red and blue vertical tick marks denote the raw data, the Rietveld refinement curve, the difference curve, and the *hkl* positions for ZIF-7 and aluminum, respectively.

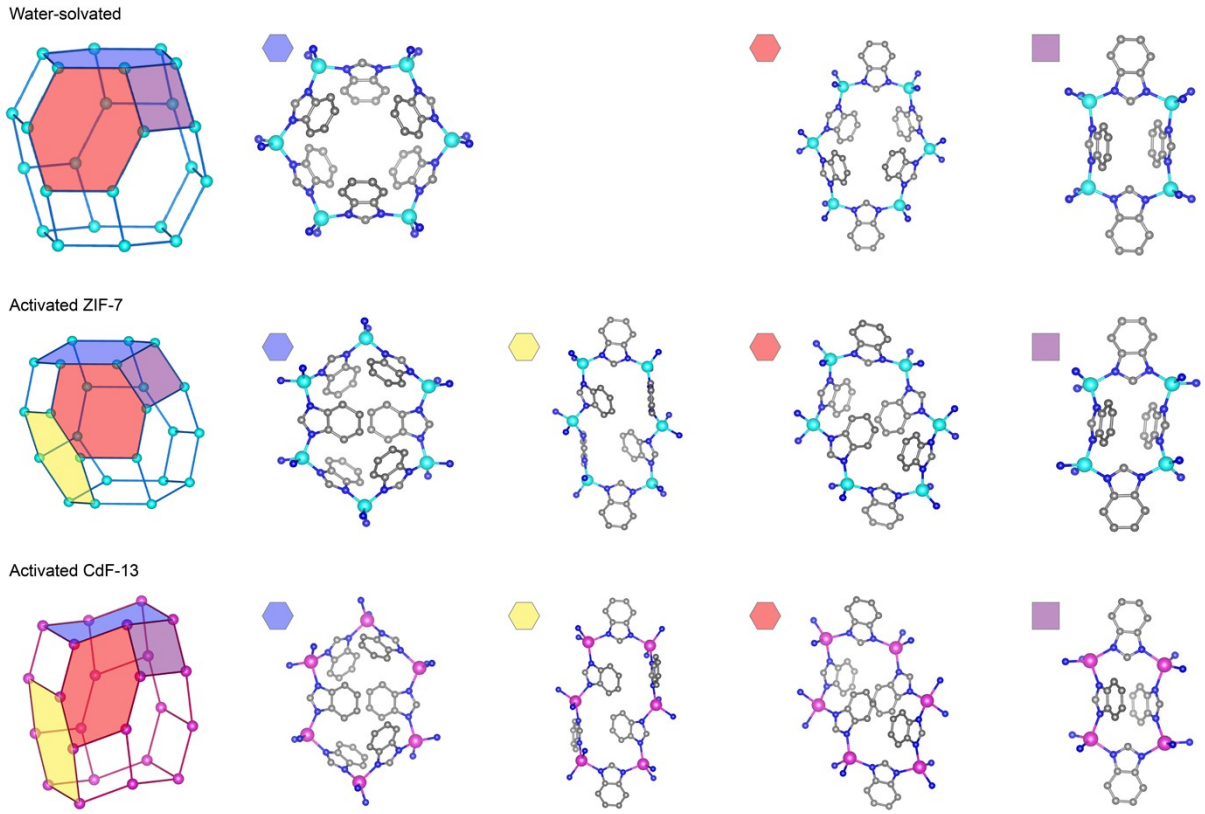

Figure S14. The structure for water-solvated ZIF-7 (top row, adapted from reference 20) is compared to the activated phases of ZIF-7 (middle row) and CdIF-13 (bottom row). The distinct rings comprising the sodalite-like topology in these materials are highlighted using different colored polygons. The distortions to the framework are more significant in activated CdIF-13 than in activated ZIF-7. However, the structures of the individual rings in these compounds are similar. Teal, pink, blue, and gray spheres depict Zn, Cd, N, and C atoms, respectively, while H atoms are omitted for clarity.

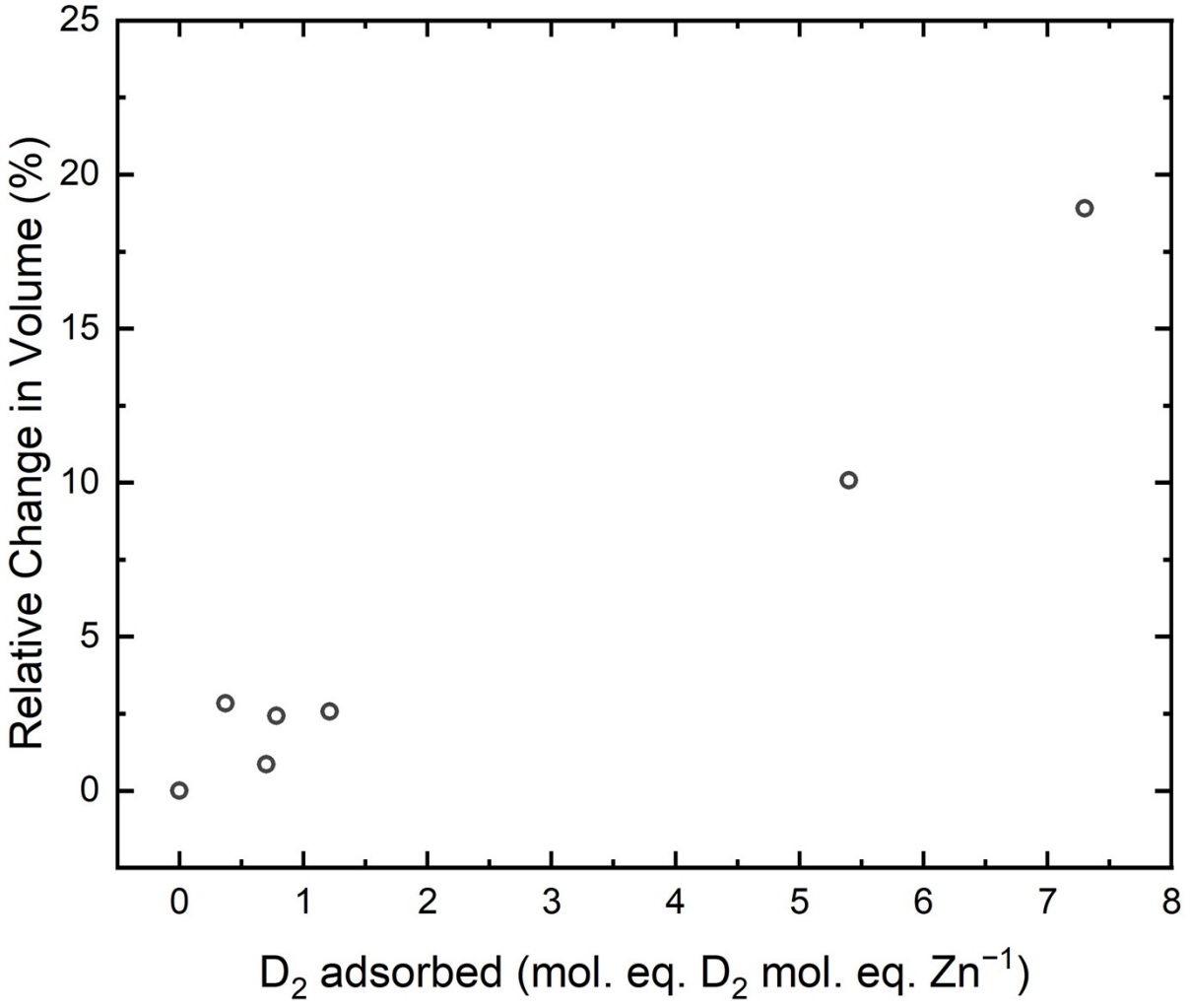

Figure S15. The approximate relative change in volume, calculated as the framework density of the D_2-dosed structures divided by the density of the activated structure, plotted as a function of D_2 loading as derived from the Rietveld refinement fits (Table S3). Note that the phase transition from the dense $P\bar{1}$ structure to the open $P2_1/n$ structure occurs between 1.21(6) eq. D_2 adsorbed and 5.4(3) eq. D_2 adsorbed. The data point at (0,0) corresponds to the activated phase.

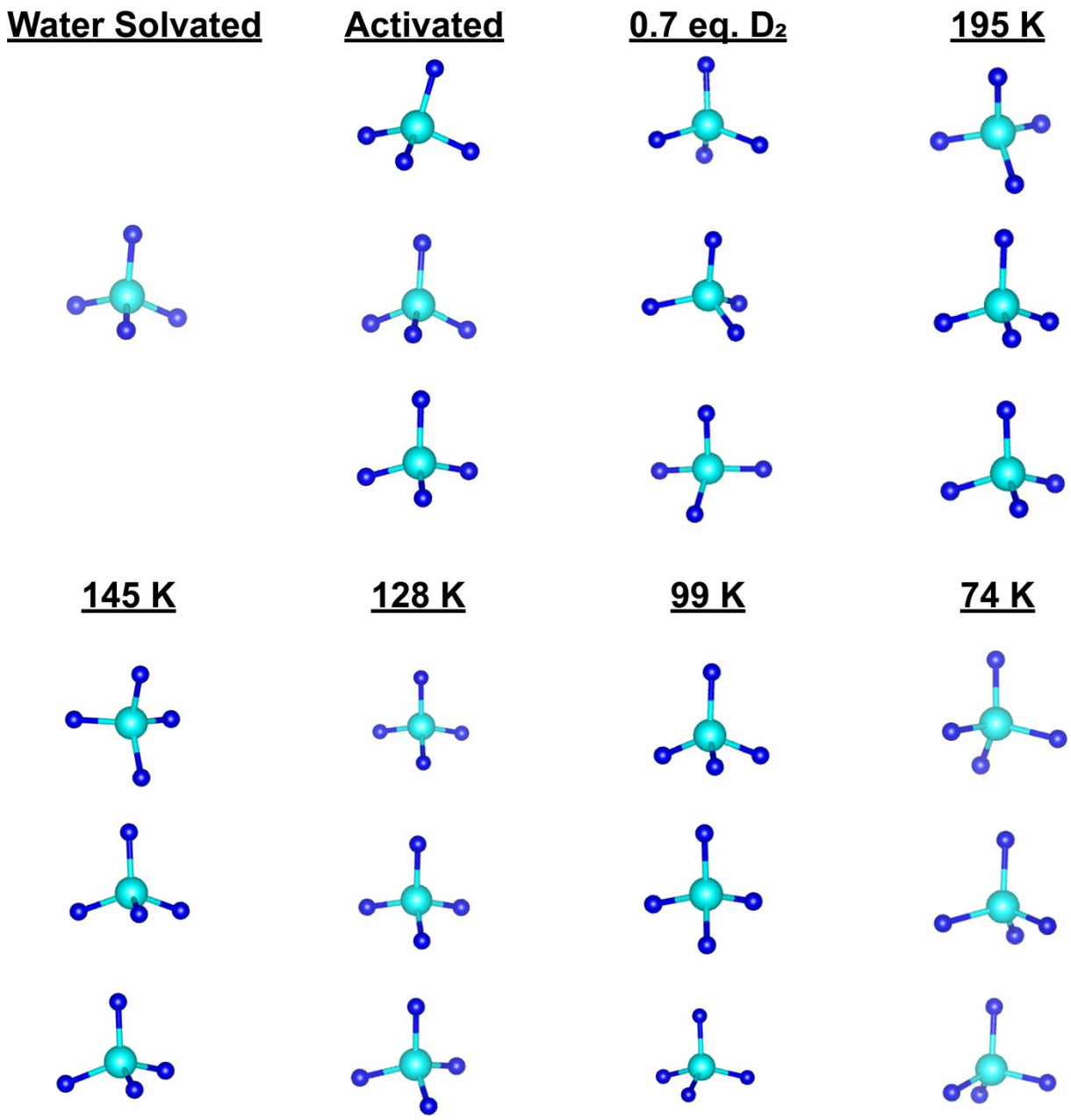

Figure S16. The $\{ZnN_4\}$ tetrahedra in the lower symmetry structures display subtle distortions relative to the high symmetry, water-solvated structure. The tetrahedron labeled as "water solvated" is adapted from reference 20. The structures are labeled based on the temperature at which they were collected for the isobaric data collection at ≈ 30 bar D_2. Blue and teal spheres depict N and Zn atoms, respectively.

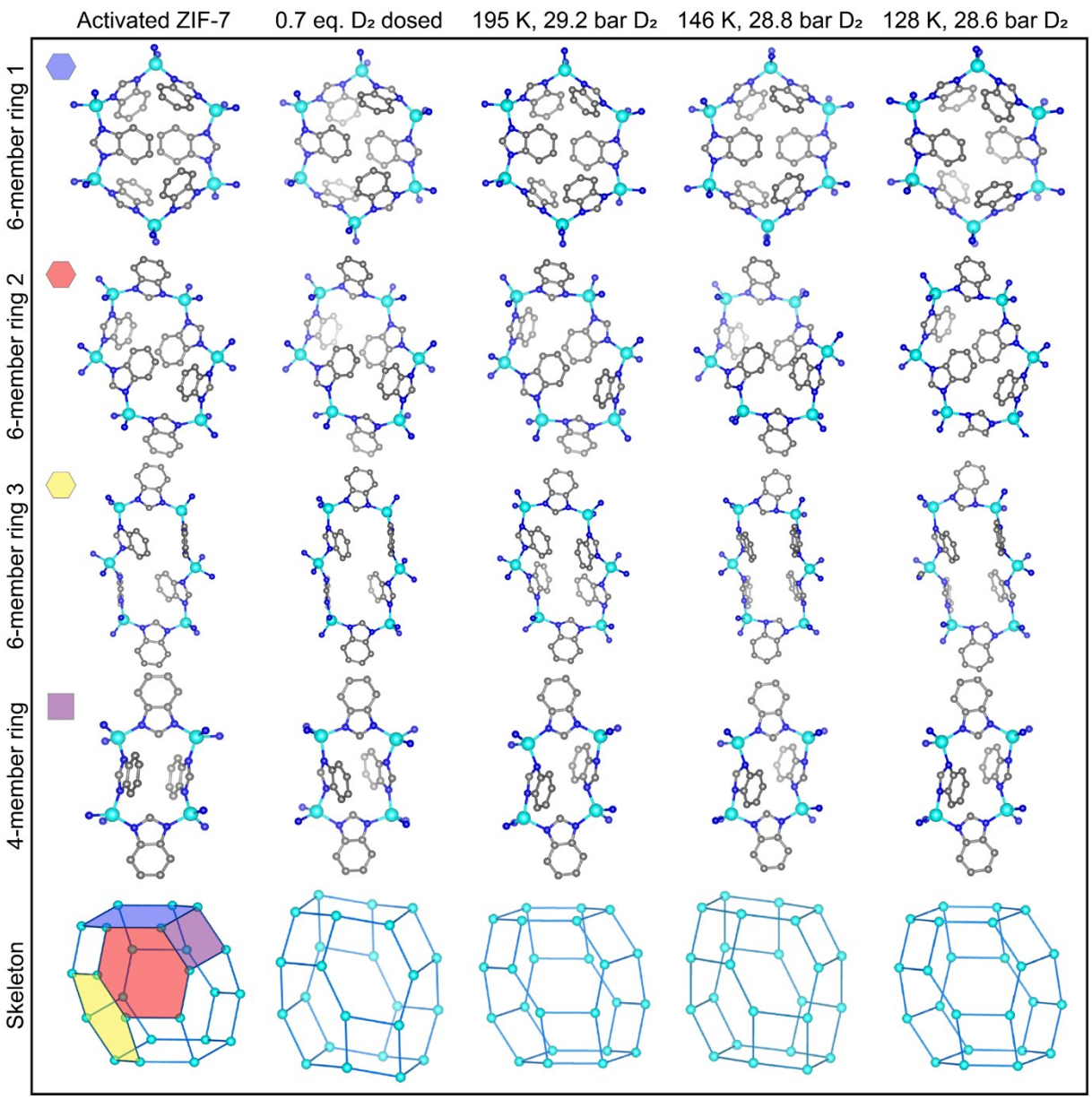

Figure S17. The rings and cages for the structures derived from Rietveld refinements of PND data obtained at 11 K, 0.7 eq. D_2 per Zn ion and at 148 K, 28.8 bar D_2 are compared here to the structures for the activated material and at two other temperatures in the pre-step regime at ~ 30 bar of D_2. Teal, gray, and blue spheres represent Zn, N, and C atoms, respectively.

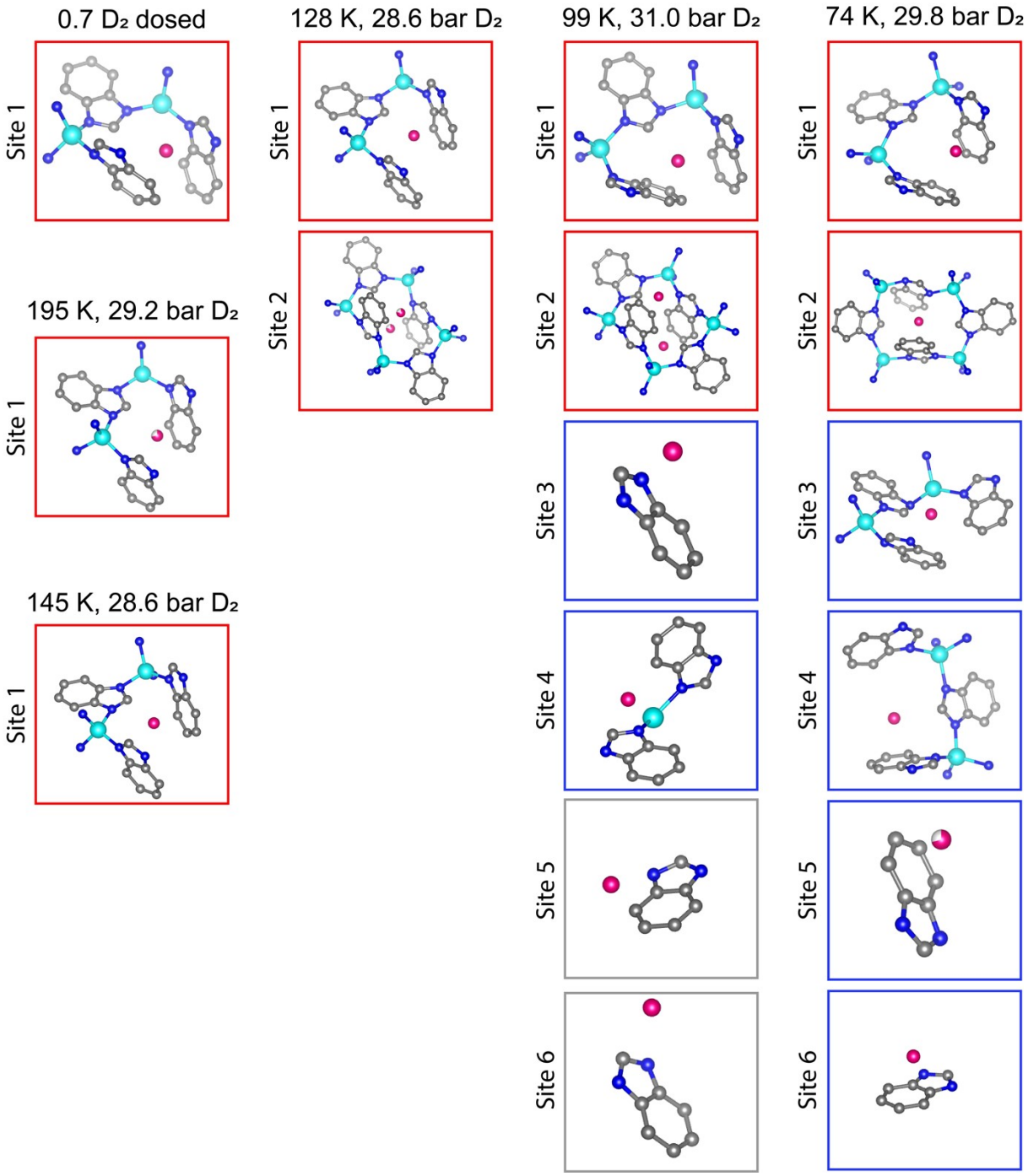

Figure S18.Sections of the reported structures are shown depicting the gas adsorption sites for D_2 dosed ZIF-7 at varying temperature and pressure conditions. The sites outlined in red illustrate sandwich-like adsorption motifs, the sites outlined in blue illustrate half sandwich-like adsorption sites, and the sites outlined in gray illustrate D_2 adsorption sites supported by van der Waals interactions with non-arene substituents in the framework. Not pictured are adsorption sites VII, VIII, and IX for the 74 K, which adsorb via longer adsorbate-adsorbate and adsorbate-adsorbent van der Waals contacts in the pores of ZIF-7. Sites are given the same number label between the different structures, but we do not mean to imply continuous occupation of that site by the same D_2 molecule across the structures. Teal, gray, blue, and pink spheres depict Zn, C, and N atoms and D_2 molecules, respectively.

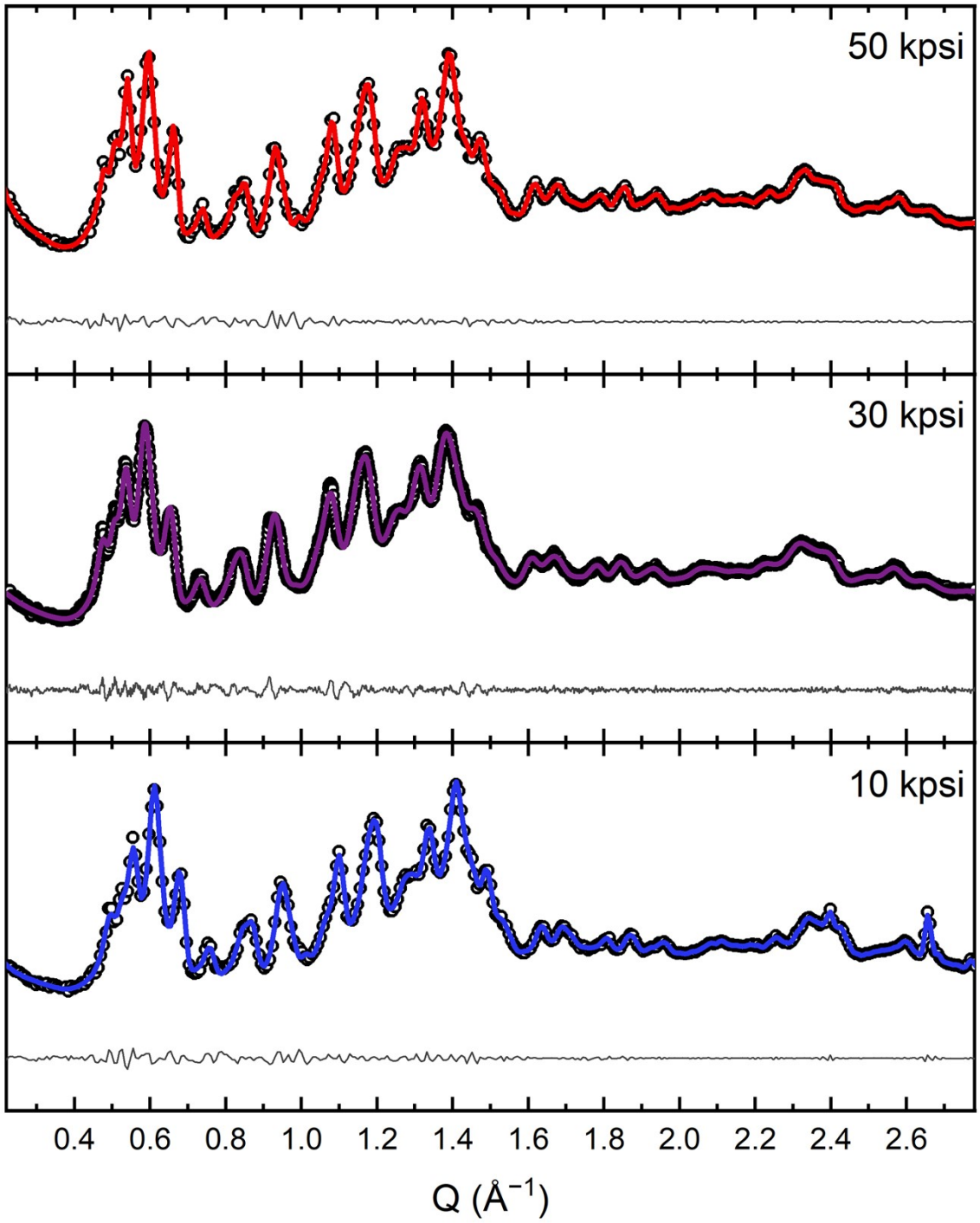

Figure S19. Powder X-ray diffraction patterns for the pelletized and activated ZIF-7. The external applied pressure used to generate each pellet is shown at the top right of each plot of the data. The black circles, colored curves, and gray curves depict the data, the Pawley fits to the data, and the difference curves, respectively. The unit cell parameters extracted from the Pawley fitting process are tabulated in Table S6 for each pellet. 10 kpsi, 30 kpsi, and 50 kpsi correspond to ≈ 690 bar, ≈ 2070 bar, and ≈ 3450 bar, respectively.

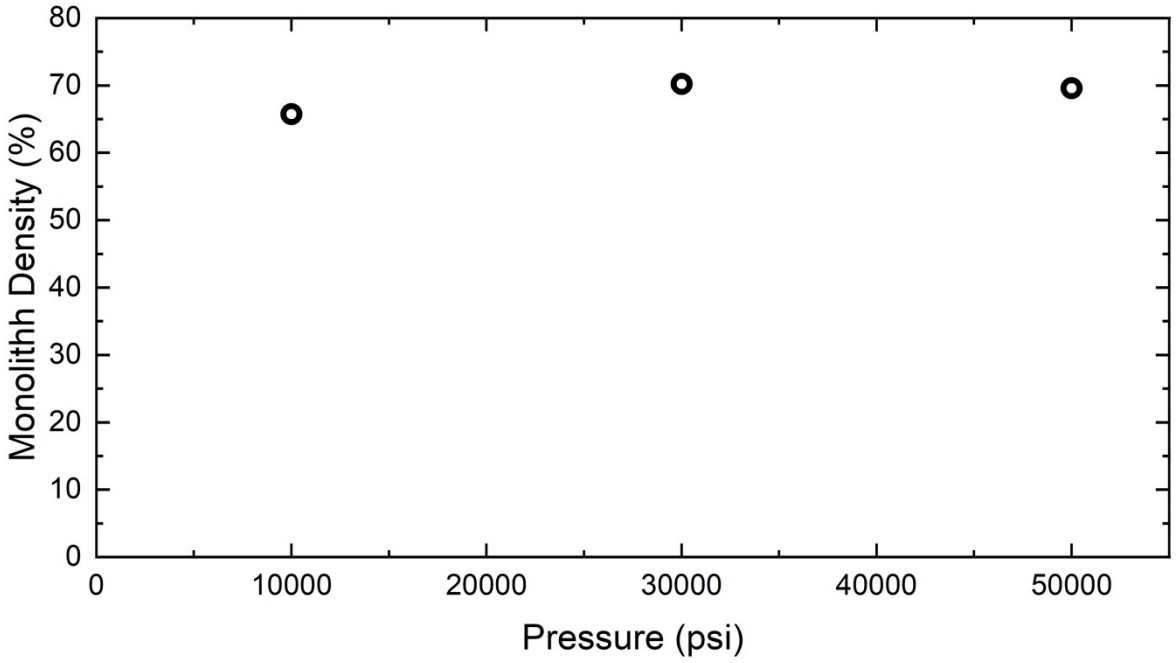

Figure S20. Monolith density vs. pressure applied for pellets produced. Monolith density calculated as the measured density of the pressed pellets multiplied by the crystal density as a percentage of the crystal density. 10 kpsi, 30 kpsi, and 50 kpsi correspond to ≈ 690 bar, ≈ 2070 bar, and ≈ 3450 bar, respectively.

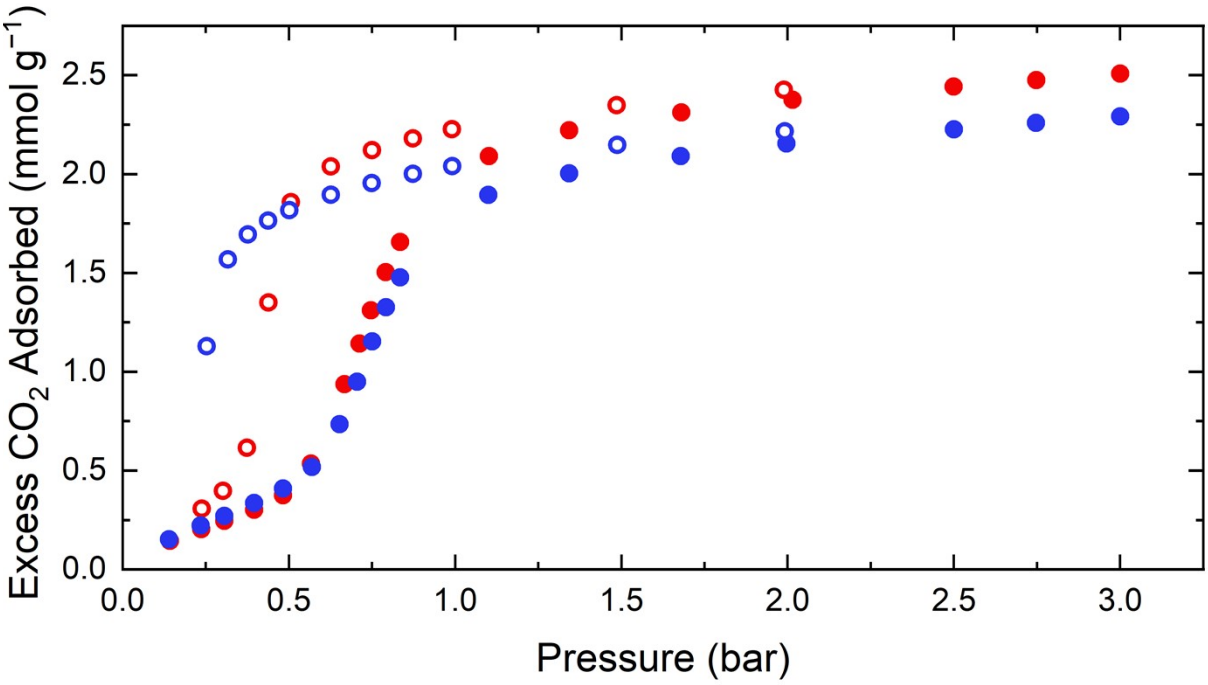

Figure S21. CO_2 isotherms of ZIF-7 powder (black) and ZIF-7 50,000 psi (≈ 3450 bar) pellet with 5 w mass % polyvinylpyrrolidone (PVP) binder (red) measured at 298 K. The closed circles denote the data collected upon adsorption and open circles denote data collected upon desorption.

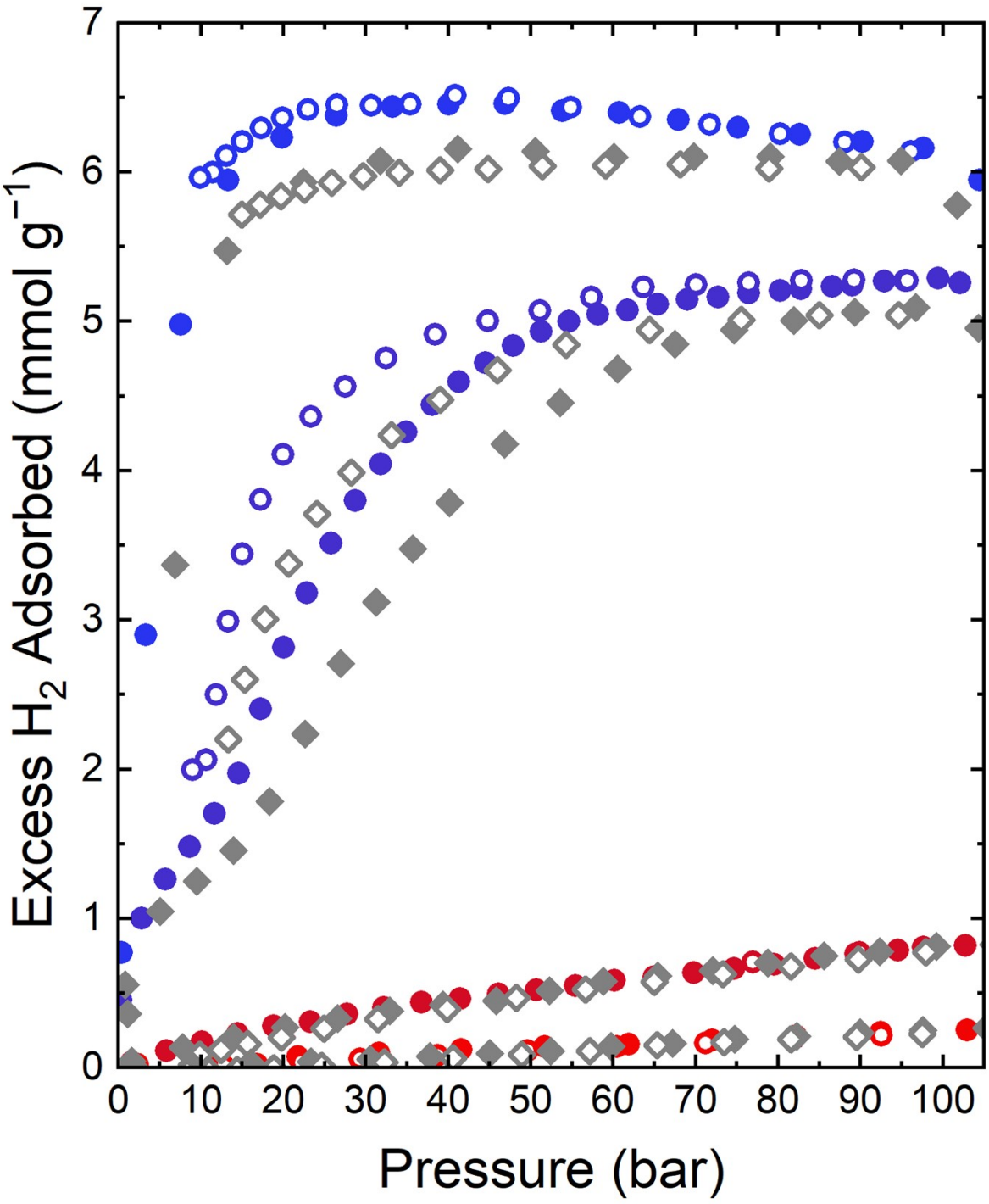

Figure S22. H_2 adsorption isotherms of ZIF-7 powder (red and blue circles) and ZIF-7 50,000 psi (≈ 3450 bar) pellet with 5 mass % polyvinylpyrrolidone (PVP) binder (gray diamonds) measured at 77 K, 100 K, 200 K, and 303 K (from top to bottom). The data for the pellet are corrected to account for the mass of the binder. The closed symbols denote the data collected upon adsorption and open symbols denote data collected upon desorption.

$$n = \frac{a(bP)^c}{1 + (bP)^c} \quad \text{(Eq. S2)}$$

Temperature	Parameter	Closed Phase	Open Phase
100 K	a	0.023274	0.017628
	b	0.0040851	0.051362
	c	0.40703	2.2425
110 K	a	0.016878	0.016473
	b	0.0073376	0.030425
	c	0.45328	2.464
125 K	a	0.021414	0.01734
	b	0.0020694	0.014058
	c	0.49056	2.2095

Table S1. Single-site Freundlich-Langmuir fit coefficients for the dense and open phases of ZIF-7 at 100 K, 110 K, and 125 K. Equation S2 is reproduced above the table for reference.

Material	*a* (Å)	*b* (Å)	*c* (Å)	α (°)	β (°)	γ (°)	Volume (Å^3)	Density (g/cm^3)	Space Group	Ref.
ZIF-7·H_2O	22.989(3)	22.989(3)	15.763(3)	90	90	120	7214(2)	1.390	$R\bar{3}$	20
CdIF-13·DMF	16.2363(6)	22.615(1)	29.909(1)	90	94.639(2)	90	10946	1.550	$P2_1/n$	2
CdIF-13·DCM	14.7241(7)	21.425(1)	17.2433(7)	90	113.366(2)	90	4993	1.666	$P2_1/n$	2
ZIF-7, 74 K, 29.8 bar D_2	14.723(6)	21.84(1)	16.169(7)	90	111.18(3)	90	4848(4)	1.272	$P2_1/n$	
ZIF-7, 99 K, 31.0 bar D_2	13.694(8)	19.565(12)	16.955(10)	90	105.86(5)	90	4370(5)	1.399	$P2_1/n$	
ZIF-7, 128 K, 28.6 bar D_2	11.599(3)	14.189(5)	14.226(5)	109.24(3)	95.73(3)	109.95(2)	2018(1)	1.488	$P\bar{1}$	
ZIF-7, 146 K, 28.8 bar D_2	11.571(3)	14.184(5)	14.249(5)	109.37(3)	95.68(3)	109.86(2)	2015(1)	1.487	$P\bar{1}$	
ZIF-7, 195 K, 29.2 bar D_2	11.569(3)	14.203(5)	14.297(5)	109.47(2)	95.70(3)	109.84(2)	2023(1)	1.478	$P\bar{1}$	
ZIF-7 activated, 10 K	11.320(3)	14.157(5)	14.213(5)	109.81(2)	95.32(2)	109.48(2)	1965.2(1)	1.519	$P\bar{1}$	
ZIF-7, 0.7 eq. D_2-dosed	11.450(3)	14.119(4)	14.191(4)	109.39(2)	95.50(2)	109.66(2)	1981.4(1)	1.511	$P\bar{1}$	
ZIF-7 activated, 300 K	23.948(6)	21.354(6)	16.349(4)	90.28(2)	93.28(2)	108.41(1)	7917(3)	1.131	$P\bar{1}$	18

Table S2. The unit cell parameters, volume, and density for the refined ZIF- structures reported here are compared to similar compounds from the literature. The error values in parentheses indicate one standard deviation. The reported crystalline densities include the adsorbate(solvent) molecules. "Ref." stands for reference number and indicates the publication from which the tabulated data were obtained. Values in parentheses indicate ±1σ.

Pressure (bar)	Temperature (K)	# D_2 from refinements	# H_2 from isotherms
29.8	74	7.3(4)	≈ 7.55
31.0	99	5.4(3)	≈ 5.63
28.6	128	1.21(6)	≈ 1.20
28.8	146	0.78(3)	≈ 0.76
29.2	195	0.37(4)	≈ 0.33
0.7 eq. D_2	11	0.70(3)	

Table S3. The refined number of D_2 molecules per Zn ion in the formula unit are compared to the number of H_2 molecules adsorbed per Zn ion in the formula unit derived from the isotherm data. The amount of H_2 derived from the isotherm measurements is extrapolated from a linear fit of data points in the isotherm data set closest in pressure to the measurement conditions of the correspond PND measurement. For the PND measurements that followed the isotherm, the overpressure in the headspace of the system is given. The stoichiometric gas dosing was done such that, upon full adsorption, the pressure in the head space was measured to be 0 mmHg (at ≈ 50 K, the temperature was then further lowered for the measurement). Values in parentheses indicate $\pm 1\sigma$.

Material	Density (g/cm^3)	Framework Density (g/cm^3)	Ref.
ZIF-7·H_2O	1.390	1.241	20
ZIF-7, Activated	1.519	1.519	
ZIF-7, Activated, 300 K	1.131	1.131	18
CdIF-13·DCM	1.666	1.383	2

Table S4. Tabulated framework densities calculated for published compounds excluding the solvent or gas molecules, compared to ZIF-7. "Ref." stands for reference number and indicates the publication from which the tabulated data were obtained.

Site #	D_2 Molecular Occupancy					
	0.7 eq. D_2	195 K	146 K	128 K	99 K	74 K
1	0.70(3)	0.37(4)	0.78(3)	0.82(2)	1.00(4)	1.00(5)
2				0.39(3)	1.00(4)	0.93(4)
3					0.81(5)	0.78(5)
4					0.78(5)	1.00(5)
5					0.83(4)	0.35(4)
6					1.00(4)	0.52(4)
7						1.00(4)
8						0.77(4)
9						1.00(5)

Table S5. Tabulated occupancies for D_2 molecules. The crystal structures are referred to by the temperature at which the data were collected at ≈ 30 bar D_2. Values in parentheses represent the estimated standard deviation. Site numberings are not necessarily consistent between structures. Values in parentheses indicate $\pm 1\sigma$.

Material	*a* (Å)	*b* (Å)	*c* (Å)	α (°)	β (°)	γ (°)	Volume (Å^3)	Source	Space Group
ZIF-7 activated, 10 K Powder	11.320(3)	14.157(5)	14.213(5)	109.81(2)	95.32(2)	109.48(2)	1965.2(1)	Neutron	$P\bar{1}$
ZIF-7, pelletized, 10 kpsi, activated	11.483(2)	14.171(2)	14.334(2)	109.93(9)	96.27(8)	109.30(9)	2003.9(5)	X-ray	$P\bar{1}$
ZIF-7, pelletized, 30 kpsi activated	11.640(2)	14.252(2)	14.387(2)	109.76(8)	96.38(1)	109.40(1)	2049.9(6)	X-ray	$P\bar{1}$
ZIF-7, pelletized, 50 kpsi activated	11.560(1)	14.296(2)	14.385(2)	109.70(8)	96.13(9)	109.59(1)	2043.2(5)	X-ray	$P\bar{1}$

Table S6. The unit cell parameters for the pelletized samples of ZIF-7 as extracted from Pawley fitting the data. 10 kpsi, 30 kpsi, and 50 kpsi correspond to ≈ 690 bar, ≈ 2070 bar, and ≈ 3450 bar, respectively. Values in parentheses indicate ±1σ.

Material	Activated CdIF-13
Empirical Formula	$C_{42}H_{30}Cd_3N_{12}$
Formula Weight ($g \cdot mol^{-1}$)	1039.98
Temperature (K)	100
Crystal System	Triclinic
Space Group	*P*-1
a, *b*, *c* (Å)	11.0002(2), 14.4168(2), 14.7647(2)
α, β, γ (°)	110.760(2), 92.6070(10), 105.591(2)
Volume ($Å^3$)	2083.00(6)
Z	2
ρ_{calc} ($g \cdot cm^{-3}$)	1.658
μ (mm^{-1})	12.518
F(000)	1020
Crystal Dimensions (mm)	0.015 x 0.041 x 0.048
2θ Range for Data Collection (°)	6 – 153
Index Ranges	$-5 \leq h \leq 13, -17 \leq k \leq 17, -17 \leq l \leq 17$
Reflections Collected	25490
Unique Data	7411 [R_{int} = 0.0537]
Data/Restraints/Parameters	7411/0/514
Goodness of Fit on F^2	1.059
Final R Factors, [I > 2σ (I)]	R_1= 0.0410 wR_2= 0.1001
Largest Residual Peak/Hole ($e \cdot Å^{-3}$)	1.796/ −0.978

Table S7. Crystallographic parameters for the single crystal structure of activated CdIF-13. Values in parentheses indicate ±1σ.

References

(1) He, M.; Yao, J.; Li, L.; Wang, K.; Chen, F.; Wang, H. *ChemPlusChem* **2013**, *78*, 1222-1225.
(2) McGuirk, C. M.; Runčevski, T.; Oktawiec, J.; Turkiewicz, A.; Taylor, M. K.; Long, J. R. *J. Am. Chem. Soc.* **2018**, *140* (46), 15924–15933.
(3) Rigaku Oxford Diffraction, (2020), CrysAlis^{Pro} Software system, version 1.171.41.63a, Rigaku Corporation, Oxford, UK.
(4) *SCALE3 ABSPACK*; A Rigaku Oxford Diffraction program (1.0.11,gui:1.0.7) (c) 2005-2020 Rigaku Oxford Diffraction.
(5) Sheldrick, G.M. *Acta Cryst.* **2015**, *A71*, 3–8.
(6) Dolomanov, O. V.; Bourhis, L. J.; Gildea, R. J.; Howard, J. A. K.; Puschmann, H. *J. Appl. Cryst.* **2009**, *42*, 339–341.
(7) Gross, K. J.; Carrington, K. R.; Barcelo, S.; Karkamkar, A.; Purewal, J.; Ma, S.; Zhou, H.-C.; Dantzer, P.; Ott, K.; Burrell, T.; Semeslberger, T.; Pivak, Y.; Dam, B.; Chandra, D. Department of Energy: Washington, D.C., 2012.
(8) McCarty, R. D.; Arp, V.; Fox, J. R. GASPAK; Cryodata, Inc., (2005). https://htess.com/gaspak/.
(9) Nash, L. K. *Elements of chemical thermodynamics*. Reading, Mass, Addison-Wesley Pub. Co, 1970.
(10) Stadie, Nicholas P. (2013) *Synthesis and Thermodynamic Studies of Physisorptive Energy Storage Materials*. Dissertation (Ph.D.), California Institute of Technology.
(11) Sincar, S. *Ind. Eng. Chem. Res.* **2018**, *57*, 6766–6773.
(12) Sips, R. *J. Chem. Phys.* **1948**, *16*, 490.
(13) Coelho, A. Topas Academic v6; Coelho Softw. (2017). http://www.topas-academic.net/.
(14) Larson, A.C.; Von Dreele, R.B. "General Structure Analysis System (GSAS)", Los Alamos National Laboratory Report LAUR, **2000**, 86–748.
(15) Toby, B. H. *J. Appl. Cryst.* **2001**, *34*, 210–213.
(16) Pawley, G. S. *J. Appl. Crystallogr.* **1981**, *14*, 357–361.
(17) Zhao, P.; Lampronti, G. I.; Lloyd, G. O.; Wharmby, M. T.; Facq, S.; Cheetham, A. K.; Redfern, S. *Chem. Mater.* **2014**, *26*, 1767–1769.
(18) Andreev, Y. G.; MacGlashan, G. S.; Bruce, P. G. *Phys. Rev. B.* **1997**, *55*, 12011–12017.
(19) Park, K. S.; Ni, Z.; Côté, A. P.; Choi, J. Y.; Huang, R.; Uribe-Romo, F. J.; Chae, H. E.; O'Keefe, M.; Yaghi, O. M. *Proc. Natl. Acad. Sci. U. S. A.* **2006**, *103*, 10186–10191.
(20) Rietveld, H. M. *J. Appl. Crystallogr.* **1969**, *2*, 65–71.
(21) Runčevski, T.; Kapelewski, M. T.; Torres-Gavosto, R. M.; Tarver, J. D.; Brown, C. M.; Long, J. R. *Chem. Comm.* **2016**, *53*, 8251–8254.
(22) Wu, H.; Zhou, W.; Yildirim, T.; *J. Am. Chem. Soc.* **2006**, *129*, 5314–5315.